Spin correlations in the extended kagome system YBaCo$_3$FeO$_7$

Martin Valldor,[1,*] Raphaël P. Hermann,[2,3] Joachim Wuttke,[4] Michaela Zamponi,[4] and Werner Schweika[2]

[1]*II. Physikalisches Institut, Universität zu Köln, D-50937 Köln, Germany*

[2]*Jülich Centre for Neutron Science (JCNS) and Peter Grünberg Institute (PGI), JARA-FIT, Forschungszentrum Jülich, 52425 Jülich, Germany*

[3]*Faculty of Science, University of Liege, 4000 Liege, Belgium*

[4]*Jülich Centre for Neutron Science (JCNS), Forschungszentrum Jülich GmbH, Outstation at FRM II, Lichtenbergstraße 1, 85747 Garching, Germany*

The transition metal-based oxide YBaCo$_3$FeO$_7$ is structurally related to the mineral *Swedenborgite* SbNaBe$_4$O$_7$, a polar noncentrosymmetric crystal system. The magnetic Co$_3$Fe sublattice consists of a tetrahedral network containing kagome-like layers with trigonal interlayer sites. This geometry causes frustration effects for magnetic ordering, which were investigated by magnetization measurements, Mössbauer spectroscopy, polarized neutron diffraction, and neutron spectroscopy. Magnetization measurement and neutron diffraction do not show long range ordering even at low temperature (1 K), although a strong antiferromagnetic coupling ($\sim$2000 K) is deduced from the magnetic susceptibility. Below 590 K we observe two features, a spontaneous weak anisotropic magnetization hysteresis along the polar crystallographic axis and a hyperfine field on the Fe kagome sites, whereas the Fe spins on the interlayer sites remain idle. Below $\sim$50 K the onset of a hyperfine field shows the development of moments static on the Mössbauer time scale also for the Fe interlayer sites. Simultaneously, an increase of spin correlations is found by polarized neutron diffraction. The relaxation part of the dynamic response has been further investigated by high-resolution neutron spectroscopy, which reveals that the spin correlations start to freeze below $\sim$50 K. Monte Carlo simulations show that the neutron scattering results at lower temperatures are compatible with a recent proposal that the particular geometric frustration in the *Swedenborgite* structure promotes quasi–one-dimensional partial order.

I. INTRODUCTION

Geometric frustration, a common phenomenon in many crystal structures, has an important effect in magnetic systems, reducing the stability of ordered antiferromagnetic states and being the origin of various examples of exotic spin physics. One of the most prominent examples of geometric frustration is the "spin-ice" property of pyrochlores (Dy$_2$Ti$_2$O$_7$), where the existence of topological magnetic monopoles has been suggested.[1–3] The typical structural features of triangle and tetrahedral networks can be found not only in pyrochlores but in many crystal structures, for example, in garnets, spinels, and in a number of kagome systems, such as the *Herbertsmithite* ZnCu$_3$(OH)$_6$Cl$_2$,[4] *Volborthite* Cu$_3$V$_2$O$_7$(OH)$_2$·2H$_2$O,[5] *Magnetoplumbite* SrCr$_{8−x}$Ga$_{4+x}$O$_{19}$,[6] and *Jarosite* (D$_3$O)Al$_3$(SO$_4$)$_2$(OD)$_6$.[7] Magnetic *Swedenborgites*, structurally related to the mineral SbNaBe$_4$O$_7$,[8–10] also belong to the class of geometrically frustrated magnets containing kagome planes in an alternating stacking with trigonal interlayer sites. According to a recent study, the neutron-diffraction patterns of Co- and Fe-based *Swedenborgites* reveal a broad spectrum of spin-freezing phenomena, ranging from long- to short-range magnetic order, i.e., from Néel states to apparent spin-liquid or spin-glass states.[11] Magnetic studies[12–14] of the compound YBaCo$_4$O$_7$ yielded partly controversial results with respect to the transition temperature and the nature of magnetic ordering. According to Chapon *et al.* magnetic long-range order occurs below 110 K,[12] whereas according to Soda *et al.*[13] and Valldor *et al.*[14] only broad magnetic peaks are observed in neutron-diffraction data due to short-range ordering of magnetic moments. Recently, Manuel *et al.*

measured the diffuse scattering from a YBaCo$_4$O$_7$ single crystal at 130 K,[15] i.e., above the ordering temperature. By comparing the observations with Monte Carlo simulations the authors argue that the system is suitably described by an isotropic nearest-neighbor Heisenberg model. Interestingly, the isotropic nearest-neighbor exchange model for the *Swedenborgite* structure results in spin correlations with strong one-dimensional (1D) character, a finding that has been confirmed in a more recent detailed study.[16] The closely related compound Y$_{0.5}$Ca$_{0.5}$BaCo$_4$O$_7$, obtained by partial substitution of the cation Y by Ca, does not show any long-range ordering down to temperatures as low as 1.2 K,[17] although the Curie-Weiss temperature is huge ($\sim$2000 K).[18] The diffuse magnetic scattering of Y$_{0.5}$Ca$_{0.5}$BaCo$_4$O$_7$ closely resembles the scattering from a well-studied model of frustration, i.e., the nearest-neighbor kagome antiferromagnet, and compares favorably well with the modeled spin correlations of decoupled two-dimensional (2D) kagome lattices. Apparently the interlayer coupling must be significantly weaker in Y$_{0.5}$Ca$_{0.5}$BaCo$_4$O$_7$ than in YBaCo$_4$O$_7$. Whereas the absence of long-range order in 2D Heisenberg antiferromagnets is in accordance with the Mermin-Wagner theorem,[19] surprisingly a complete suppression of long-range order in three-dimensional (3D) coupled spin systems was also found in recent model calculations.[16] Apparently in the case of 3D coupling the disordered ground state has to be attributed to unusually strong geometric frustration effects, which are different from site- or bond-disorder, the typical ingredients for spin-glass formation.[20]

An alternate model, including 3D spin correlations, has been proposed[21] that provides preliminary insights into the

spin dynamics. Two components are observed in neutron spectroscopy. One of these corresponds to slow spin relaxations and indicates a freezing of spin configurations below approximately 50 K. The dynamical response related to the second component is temperature independent and corresponds to fast spin relaxations. However, to date, neither structural investigations nor the first results on the spin dynamics in the *Swedenborgites* have delivered a sufficiently consistent understanding.

The substitution of the magnetic ions, for example Co by Fe, provides a further degree of freedom. According to powder neutron diffraction, the compound $YBaCo_3FeO_7$ does not show an ordered magnetic ground state.[11] This new system is of particular interest because large and phase-pure single crystals can be readily grown, as will be reported subsequently.

An extensive structural description of $YBaCo_3FeO_7$ was first reported elsewhere,[22] and only a brief description is given here in order to support the understanding of the following results. The atomic ordering in the title compound can be described in two distinct ways, starting either from the (i) anions or (ii) cations. (i) BaO_7 densely packs with the *ABAC* layer ordering, leaving Ba twelve coordinated. Embedded in the oxygen sublattice, the octahedral sites are occupied by Y and tetrahedral sites are filled with Co or Fe [Fig. 1(a)]. Three quarters of the Co,Fe sites constitute *kagome* layers separated by the remaining interlayer sites. (ii) Considering only the cations, it is interesting to see that the metal sites are closely related to the Laves phases (AB_2), where YBa occupy the *A* sites and Co_3Fe the *B* sites. Hence, a better description of the *Swedenborgite* structure is the close packing of cations [Fig. 1(b)], according to Laves,[23] where the voids are filled with oxygen anions.

In this paper a suite of experimental methods comprising Mössbauer spectroscopy, x-ray and neutron scattering on polycrystalline samples, and magnetization measurements on single crystals have been applied to investigate the *Swedenborgite* $YBaCo_3FeO_7$, providing new insights into unusual and complex spin correlations, the observation of weak spontaneous spin anisotropy of the kagome spins, and a spin-glasslike freezing induced by the onset of spin correlations involving the interlayer sites at low temperatures.

II. SAMPLE CHARACTERIZATION AND EXPERIMENTAL METHODS

Polycrystalline samples were made from a stoichiometric mixture of Y_2O_3 (Alfa Aesar 99.99%), $BaCO_3$ (Strem Chem. 99.9%), Co_3O_4 (Alfa Aesar 99.7%), and Fe_2O_3 (Sigma-Aldrich +99%). After mixing the constituents in an agate mortar, the powder was heated twice at $1100\,°C$ in air in a corundum crucible with an intermediate grinding. A second sample was synthesized using $^{57}Fe_2O_3$ (>95% isotope pure). A Pt crucible was used as a reaction vessel for the synthesis of this isotope-enriched powder, but the heating procedure was the same. Large single crystals were synthesized in a floating-zone mirror-image furnace (FZ-T-10000-H-VI-VP). The polycrystalline seed and feeding rods were heated overnight in a corundum crucible in air at $1100\,°C$ in order to ensure mechanical stability. A steady flow of pure Ar
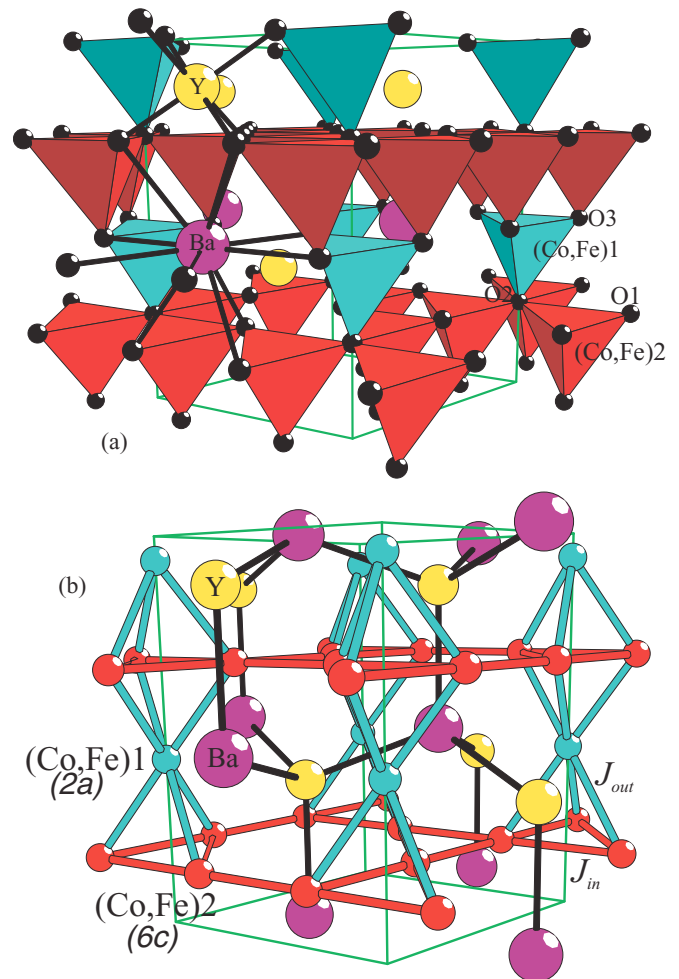

FIG. 1. (Color online) (a) Polyhedral representation of the hexagonal *Swedenborgite* ($P6_3mc$) $YBaCo_3FeO_7$ structure. The oxygen (black) at the corner of the Co,Fe containing tetrahedra are also labeled O1–O3, representing three crystallographically different sites. The coordinations of Ba and Y are indicated with black lines and the unit cell in green/gray. (b) The same structure as in (a) but without oxygen atoms, and the *kagome* sublattice is highlighted with dark bonds (red/dark gray); the brighter bonds (blue/medium gray) mark the interlayer couplings. The Wyckoff labels for the transition metal sites are stated within parentheses. A Y,Ba substructure has been created with thin bonds to emphasize the similarity between the cationic structure in *Swedenborgites* and the close packed Laves phases.

(5 cm^3/min) and growth rates between 2 and 10 mm/h were used during the crystal growth process.

The oxygen content of the resulting crystal was investigated indirectly by analyzing the oxidation states of the transition metal ions by x-ray absorption spectroscopy: only Co^{2+} and Fe^{3+} were found,[24] confirming the stoichiometric oxygen content of $O_{7.00(3)}$, as the pristine oxidation states Y^{3+} and Ba^{2+} are expected to be present in the crystal due to their high stability.

Powder x-ray diffraction (XRD) was performed with a STOE STADI P in Bragg-Brentano geometry (θ-2θ) using Cu $K\alpha_{1,2}$ radiation ($\lambda = 1.54056, 1.54439$ Å) and a position sensitive detector.

All diffraction intensities in the data from the ground single crystal sample can be indexed with the previously reported
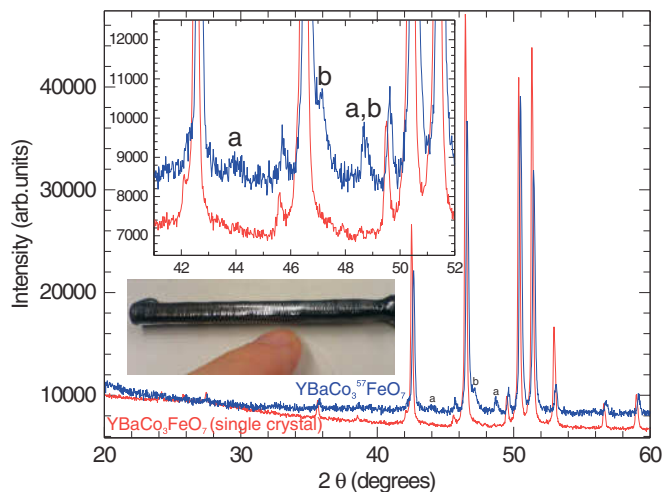
FIG. 2. (Color online) X-ray powder diffraction from a ground part of the single crystal (red/dark gray lines) and the iron-57 enriched sample (blue/medium gray lines). The inset shows small peaks from two different impurities, designated a (Y_2O_3) and b ($YBa(Co,Fe)_2O_5$). A photo of the single crystal is added as inset and a finger is present for size comparison.

hexagonal cell.[22] Due to the small size of the sample for the Mössbauer spectroscopy measurement and the uncertain reactivity of $^{57}Fe_2O_3$ (≈ 60 mg), small amounts of impurities are present in the powder sample (Fig. 2), which could be explained by a few percent of unreacted Y_2O_3 and the layered perovskite $YBa(Co,Fe)_2O_5$. It should be noted that the single crystal sample ($a = 6.32261(3)$, $c = 10.2843(1)$ Å) seems to have slightly larger unit cell parameters as the diffraction intensities are shifted to lower angles relative to the isotope sample ($a = 6.3165(4)$, $c = 10.2749(7)$ Å); the reason for this is not clear. Hence, the magnetization measurements and Mössbauer spectroscopy presented subsequently were performed on both samples. The relative Bragg intensity differences are most probably due to a preferred orientation of the crystals in the powdered single crystalline sample.

Magnetic investigations were carried out using a vibrating sample magnetometer inside a physical property measurement system (VSM-PPMS, Quantum Design) with fields of up to 1 T in the temperature range 2–1000 K with two different sample holders for either high (300–1000 K) or low temperatures (2–350 K). Zero-field cooling (ZFC) data was obtained by cooling the sample from the highest temperature to the lowest, before applying a measuring field. Accordingly, in field cooling (FC), the sample was exposed to the measuring field during lowering the temperature. All measurements were done on heating. The magnetic relaxation measurement followed a FC with 0.1 T from 650 down to 570 K. Subsequently the field was shut off and the magnetization in the sample was monitored as function of time.

Mössbauer spectra were recorded on a constant acceleration spectrometer using a 50 mCi $^{57}Co@Rh$ source calibrated with α-iron at 298 K. Spectra below room temperature were obtained with the sample in a helium flow cryostat having a temperature accuracy better than 1%. Spectra between 295 and 480 K were recorded from a 12 mg/cm^2 sample mixed with BN in a furnace, with a temperature accuracy of $\sim$5 K calibrated

to the α-iron isomer shift. In order to assess the influence of thickness broadening, a second sample with 60 mg/cm^2 of natural isotopic abundance was prepared, and spectra were recorded at 4.2 and 85 K.

Neutron diffraction with polarization analysis was performed at the Diffuse Neutron Scattering (DNS) instrument[25] of the Jülich Centre for Neutron Science (JCNS), outstation FRM II, Munich, Germany. Polarized neutrons with a wavelength of 4.75 Å have been used with subsequent XYZ-polarization analysis[26] in order to separate the magnetic scattering from the structural diffraction. A 30 g powdered single crystal sample was studied between 1.2 and 300 K.

The spin dynamics and relaxation has been studied by neutron spectroscopy using the backscattering instruments BASIS (SNS, Oak Ridge National Laboratory)[27] and SPHERES (FRMII, Munich, Germany).[28] BASIS is a time-of-flight backscattering spectrometer, where a dynamic range of ± 100 μeV has been studied with an energy resolution of 3.5 μeV full-width half-maximum (FWHM). SPHERES is a pure backscattering spectrometer with a dynamic range of ± 31 μeV and a typical resolution of 0.67 μeV (FWHM). To improve statistics near the elastic line, we used the instrument with a reduced dynamic range of ± 10.5 μeV. The Q-range of both instruments is set by the Si-111 analyser crystals to ~ 1.8 Å^{-1}. Measurements on powder samples have been taken at various temperatures below 100 K.

All in all, three samples were investigated throughout this paper: single crystalline $YBaCo_3FeO_7$ (Sec. III A), a powder from the same single crystal (XRD, IIIB, IIIC, IIID), and an isotope-enriched $YBaCo_3{}^{57}FeO_7$ powder sample (XRD, IIIA, IIIB).

III. EXPERIMENTAL RESULTS

A. Magnetic investigations

All orientation-dependent magnetic susceptibilities (χ) of $YBaCo_3FeO_7$ were extracted from a single crystalline sample, and the data are shown in Fig. 3.

At temperatures above 600 K up to 1000 K (the highest accessible temperature), the inverse susceptibility exhibits a linear decrease indicating paramagnetic-like behavior [inset Fig. 3(a)]. Applying the Curie-Weiss law at highest temperatures, i.e., between 900 and 1000 K for the low field (50 mT) data, one obtains a Curie-Weiss temperature, $\theta_{CW} = -2.0 \times 10^3$ K and a total effective magnetic moment, $M_{Co,Fe} = 14.5$ μ_B per formula unit. When taking into account only spin moments, the magnetic moment for Co^{2+} and Fe^{3+} high spin ions is 17.54 μ_B, which shows a noticeable discrepancy from the Curie-Weiss estimate. The caveat is that the estimated values of $M_{Co,Fe}$ and θ_{CW} may be affected by relatively large systematic errors because the Curie-Weiss law is expected to be valid in the limit of $T > |\theta_{CW}|$, i.e., above the accessible temperature range.

Near 590 K (T_{f1}), there is an obvious transition from isotropic to a weak anisotropic magnetic behavior for the two measured crystallographic directions. On cooling, χ increases more strongly along the unique axis (c) than perpendicular to it. Below T_{f1} FC data and ZFC data measured in $B = 1$ T perfectly superimpose. This agrees with the magnetization measurements, discussed subsequently, where
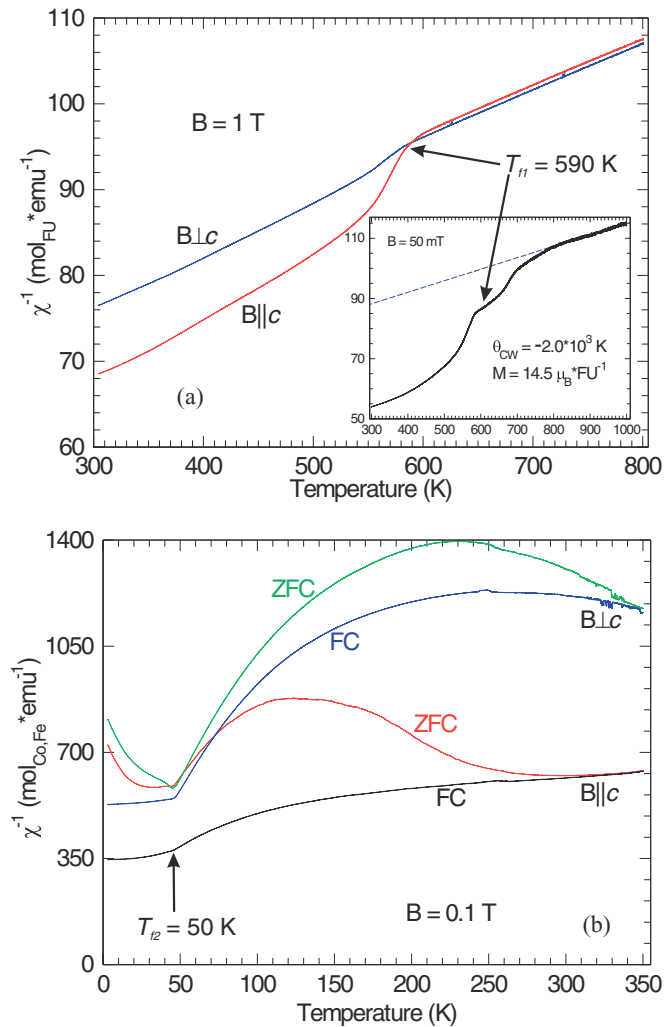
FIG. 3. (Color online) Temperature-dependent inverse magnetic susceptibility (χ^{-1}) of $YBaCo_3FeO_7$ at (a) high and (b) low temperatures. The curves are indicated with $B\|c$ if the magnetic field was applied parallel to the c-axis and $B\perp c$ if perpendicular. Both field cooled (FC) and zero-field cooled (ZFC) data are presented at all temperatures. The inset shows the inverse susceptibility data at a smaller field of 50 mT extending to 1000 K. The dashed line represents a Curie-Weiss extrapolation from the data between 900 and 1000 K.

FIG. 4. (Color online) Field-dependent magnetization in μ_B per formula unit (FU) of $YBaCo_3FeO_7$ at several temperatures and with (a) the applied field parallel ($B\|c$) and (b) perpendicular ($B\perp c$) to the c-axis. The inset in (a) exhibits measurements at lower temperatures, and the inset in (b) displays the different behaviors depending on field direction at 560 K.

the weak ferromagnetic moment has a coercive field smaller than 0.1 T. The small increase in χ with $B\perp c$ is likely to arise from a slight misalignment of the single crystal, as a resulting magnetic moment perpendicular to c is prohibited by the hexagonal symmetry. Magnetic relaxation measurements at 560 K, not shown, gave no indications of a glassy state. We note that for the ^{57}Fe-enriched Mössbauer sample, χ in a low DC field (not shown) also displays the magnetic transition at 590 K, which enables the combination of data from isotope enriched and single crystalline samples.

Considering the low temperature data, shown in Fig. 3(b), the relevance of the magnetic history of the sample is obvious, which prevents a quantitative discussion. However, close to 50 K (T_{f2}) a second anomaly with a splitting of FC and the
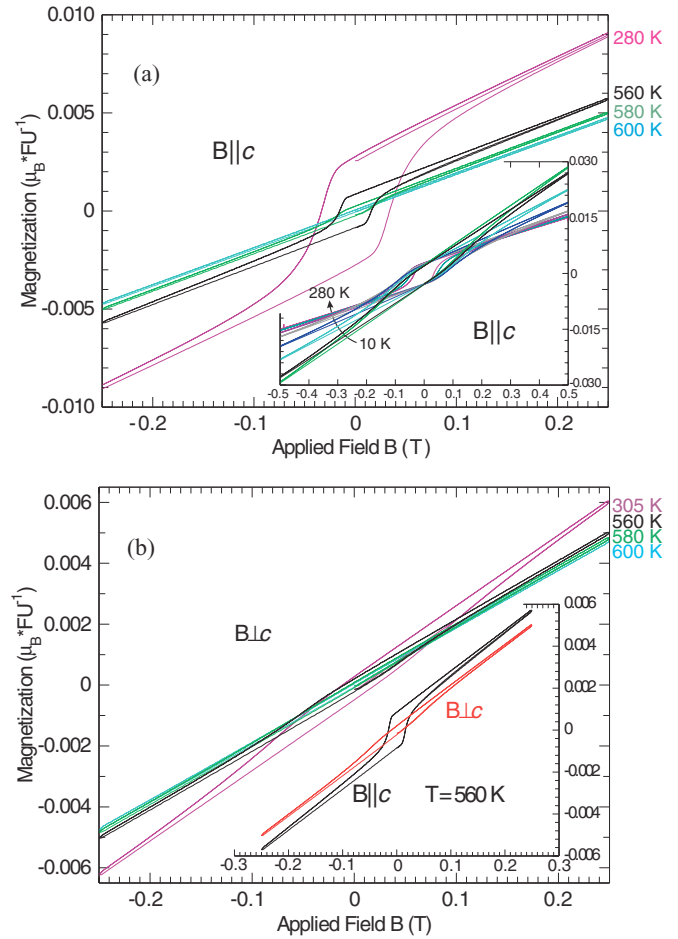
ZFC data indicates a further magnetic transition to a glassylike magnetic state.

The magnetization as function of field was measured at different temperatures both with the applied field parallel and perpendicular to the crystallographic c-axis (Fig. 4). For $B\|c$ all data below 590 K reveal a weak magnetic hysteresis [Fig. 4(a)] with an increasing coercive field down to 280 K, a coercive field that, even at lower temperatures, stays almost constant [inset in Fig. 4(a)]. At low temperatures, these hystereses loose their defined shape but have almost the same isothermal magnetic remanence. As the field was scanned at the same rate at all temperature, this behavior corresponds to a ferromagnetic component along c below 590 K, which gradually becomes viscous with decreasing temperature. In contrast the hysteresis is absent if the field is applied perpendicular to the c-axis [Fig. 4(b)], except for a small anomaly most likely resulting from a minor misalignment of the crystal. A direct comparison of data from 560 K for both field directions is shown in inset Fig. 4(b) to illustrate the anisotropy of the hysteresis. In all applied fields the induced magnetization is relatively low in agreement with

the large negative Curie-Weiss temperature and the related strong antiferromagnetic exchange.

Note that the lack of inversion symmetry in the *Swedenborgite* structure allows for Dzyaloshinsky-Moriya (DM) interactions.[29,30] DM interactions provide a possible explanation for the observed anisotropy and the magnetization hysteresis, where the induced weak ferromagnetic component can correspond to a small spin canting along the structural polar axis.

B. Mössbauer spectroscopy

The 4.2 K Mössbauer spectrum [Fig. 5(a)] reveals two distinct magnetic sublattices with hyperfine fields of 53 and 43 T. Upon heating, the subspectrum with the smallest field reveals a transition to a paramagnetic state above 50 K and that with the largest field reveals a gradual decrease of the hyperfine field up to 480 K. These observations are consistent with the magnetic susceptibility data that reveal a transition around 50 K and a second transition at 590 K. The spectral areas at 4.2 K indicate that 17(2)% of Fe is located on the site with the larger hyperfine field. A Mössbauer spectrum, not shown, recorded at 4.2 K on a thin non iron-57 enriched sample reveals a similar preferential occupation of 19(2)%. The spectral areas determine the Fe occupancies for the two sites. The assignment for the Fe occupation is made on the basis of XRD on this and isostructural compounds,[22] which show that the trivalent ions preferentially occupy the relatively smaller site 1. Accordingly, the occupations are 82(2)% Fe on the site (Co,Fe)1 and 6(1)% Fe on the three kagome plane sites (Co,Fe)2. Neither are superstructure reflections seen in, nor can short-range ordering be concluded from the neutron-diffraction experiments. For simplicity we have assumed a random Fe distribution with the given site occupations for the modeling. However, because of the different valence of Co^{2+} and Fe^{3+},[24] one may expect a preference for unlike neighbors in the kagome plane.

The Mössbauer spectra between 4.2 and 480 K were fitted with a model that includes the following components: two (Co,Fe)2 sextets, two (Co,Fe)1 sextets below 60 K, two (Co,Fe)1 doublets at and above 60 K, and one small impurity sextet with only 2.5% spectral area. We cannot identify this impurity explicitly, but we tentatively propose $YBa(Co,Fe)_2O_5$ because the hyperfine field and its temperature dependence (ca. 55 T at 4.2 and ca. 38 T at 480 K) are similar to what is observed in $TbBaFe_2O_5$[31] and are not compatible with a possible α-Fe_2O_3 impurity retained from the starting material. Moreover, this would agree with the observations from the XRD data, as only the enriched sample contains this impurity. The (Co,Fe)1 and (Co,Fe)2 sextets are broadened, and two components are required, which can be attributed to a distribution of the hyperfine fields associated with the binomial distribution of Fe at the two sites. The spectra are not sufficiently resolved to warrant a fit by a binominal distribution; instead, an incremental line-width broadening for the magnetic components was applied. For the (Co,Fe)1 site it was necessary to model the subspectrum with two broadened doublets in the high temperature phase, which is likely caused both by environment distribution and by thickness broadening as the absorption reaches 30% for the paramagnetic signal. The reported hyperfine field [Fig. 5(b)] and quadrupole shifts, see further discussion, are the weighted averages.
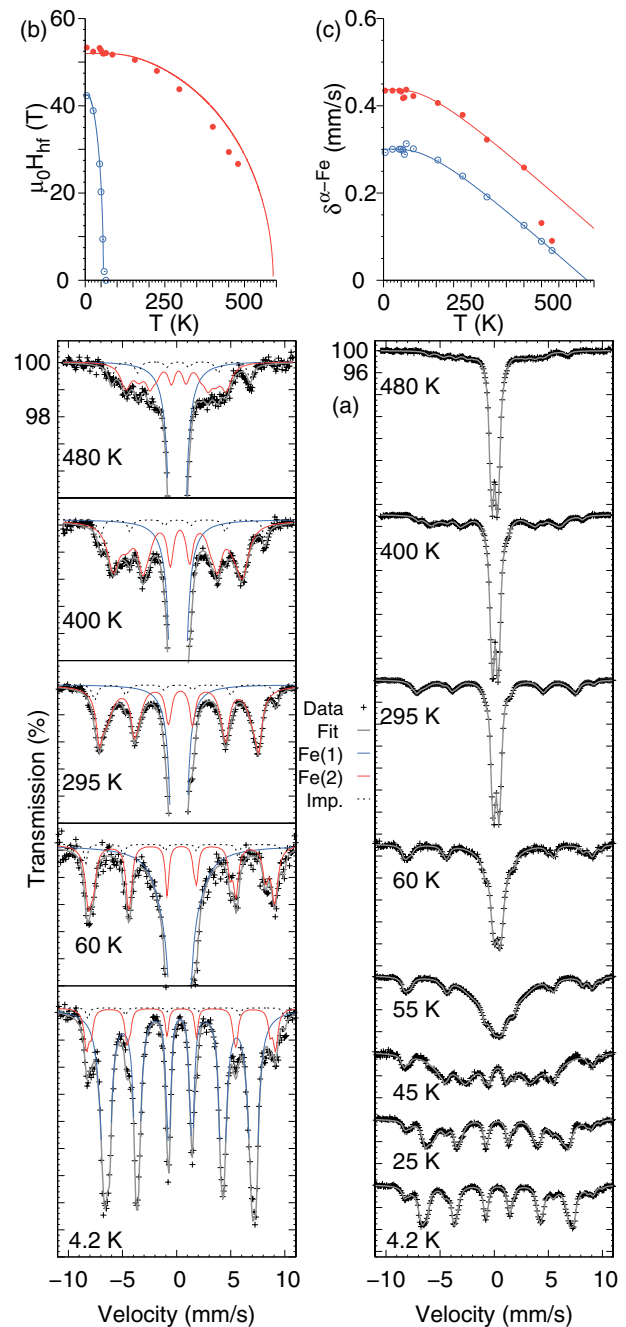

FIG. 5. (Color online) (a) Mössbauer spectra from $YBaCo_3{}^{57}FeO_7$ at selected temperatures. The (Co,Fe)1 subspectrum fit is indicated in blue/medium gray and the (Co,Fe)2 in red/dark gray. The total fit corresponds to the gray line, and the minor impurity component to the dotted line. Spectra in the left panel are vertically enlarged in order to better display the magnetic subspectra. The temperature dependence of the hyperfine field (b) and the isomer shift (c) for both sublattices are shown in blue (Co,Fe)1 and red (Co,Fe)2.

The isomer shift of the (Co,Fe)1 site in Fig. 5(c) was fitted with a Debye model, and the associated Lamb-Mössbauer temperature is $\Theta_{LM} = 440(25)$ K. A similar fit of the (Co,Fe)2 site isomer shift, up to 400 K, indicates a significantly lower $\Theta_{LM} = 240(60)$ K, and the variation of the isomer shift above 400 K is anomalous. This large difference in the Θ_{LM} is

surprising considering that the oxygen coordination of both sites is tetrahedral. The quadrupole shifts for the magnetic subspectra are essentially temperature independent: $QS_{Fe(1)} = -0.06(2)$ mm/s and $QS_{Fe(2)} = -0.11(4)$ mm/s. The average quadrupole splitting of the (Co,Fe)1 site in the paramagnetic phase is $\Delta E_Q = 0.57(2)$ mm/s. The temperature dependences of the hyperfine field for both sites are roughly consistent with a mean-field model, displayed by lines in Fig. 5(b), for a spin $J = 5/2$ and a critical temperature $T_{f2} = 55$ K and $T_{f1} = 590$ K, see blue and red lines, respectively. Note the acceptable agreement even though these curves are not fitted to the data.

The spectral parameters for the (Co,Fe)1 and (Co,Fe)2 components are typical for high-spin Fe^{3+} in oxygen environment and compatible with tetrahedral coordination, although the quadrupole splitting for the (Co,Fe)1 site is somewhat smaller than is observed in the paramagnetic spectra of iron garnets.[32] None of the recorded spectra is indicative of localized magnetic fluctuations. Hence, if fluctuations are present, they must be slower than the detection limit of ca. 1 MHz for Mössbauer spectroscopy. The observation of a magnetic subspectrum for the (Co,Fe)2 site up to 480 K is consistent with the enhanced magnetic susceptibility observed below 590 K. The hyperfine field for Fe(1) is ~10 T smaller than for Fe(2), which from a simple proportionality would indicate a ~1 μB smaller moment of ~4 μB for Fe(1) than the ~5 μB for Fe(2). Proportionality does not hold, however, as the hyperfine field is the sum of a possible orbital term, a dipolar term, and a Fermi-contact term. The near-neighbor environment for Fe(1) and Fe(2) are very similar with nearly tetrahedrally coordinating oxygen. We thus ascribe the ~10 T difference mainly to different dipolar contributions resulting from different magnetic neighbors, as the orbital term is null for high-spin Fe^{3+}, and the Fermi-contact term should be very similar for two-spin 5/2 iron with so similar coordination.

Between these two magnetic anomalies (50–590 K), the following observations are made: The macroscopic magnetization data, corresponding to large time scales (Hz), exhibit a hysteretic low moment of about 0.01 μB per formula unit along the crystallographic c-direction. The Mössbauer spectral data indicate a clear preference of Co^{2+} and Fe^{3+} ions for the kagome and interlayer sites, respectively. Above approximately 590 K, vanishing hyperfine fields suggest that all spins are paramagnetic. Below this anomaly, the observed anisotropy in magnetization relates to the appearance hyperfine fields on Fe^{3+} kagome spins. With respect to the local sensitivity of the technique we can infer local moments, which are sufficiently static to impose a Zeeman splitting of the nuclear moments. The question whether this behavior is shared by the majority of the Co^{2+} kagome spins cannot be clarified with the present data. The simultaneous onset of anisotropy, of weak magnetization hysteresis, and of hyperfine fields is remarkable, and its origin is not yet clear. Long-range magnetic order, as well as any static strong spin correlations at such high temperatures, can be ruled out by the neutron scattering results, as will be further discussed.

C. Diffuse polarized-neutron scattering

Diffuse polarized-neutron diffraction has been applied to study spin correlations and possible magnetic ordering at lower
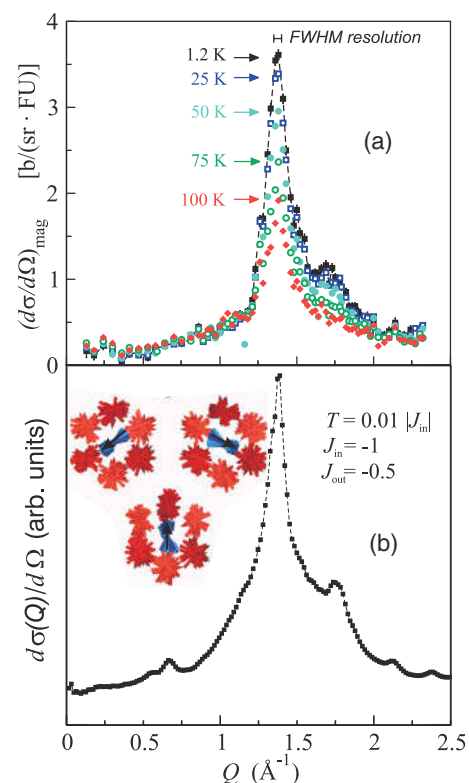

FIG. 6. (Color online) (a) Temperature and wave-vector dependence of the diffuse magnetic neutron scattering from a $YBaCo_3FeO_7$ powder sample. The separation of magnetic scattering is obtained by polarization analysis at the DNS instrument. A diffuse peak near $Q = 1.37$ Å^{-1} and second peak near $Q = 1.73$ Å^{-1} evolves upon cooling. The finite width indicates short-range correlations rather than 3D ordering at low T. The intensity increase is most likely due to the onset of strong spin correlations perpendicular to the kagome layers (see text). (b) Monte Carlo simulations based on a Heisenberg model, where $J_{out} = 0.5 \, J_{in}$ for low temperatures, $T = 0.01 \, J_{in}$. The inset shows a projection along c of a small part of the calculated spin arrangement. The two red/dark gray colors denote the spins in the alternating *kagome* layers, the blue/medium gray colors the spins at trigonal interlayer sites. Spins on the trigonal sites (blue/medium gray) show 1D ordering along the c-axis. In the ab-plane, a local ordering with ~120° angles can be seen between the (blue/medium gray) spins on trigonal sites as well as between the mediating kagome spins, which is emphasized by the (dark blue/black) spins of the top kagome layer.

temperatures. The magnetic scattering [see Fig. 6(a)] has been obtained by polarization analysis. The data were calibrated by the separated isotropic spin-incoherent scattering from the Co ions. One may note that polarization analysis also provides a separation of the nuclear coherent scattering, which includes the atomic Fe-Co short-range order. However, in contrast to the magnetic short-range order, the atomic short-range order cannot be retrieved reliably from the powder data due to additional background and diffuse scattering from lattice displacements.

The most remarkable feature of the magnetic scattering is its wave-vector dependence at lower temperatures. The observed peaks are broad and diffuse, indicating short-range magnetic correlations rather than long-range magnetic order. With decreasing temperature the dominant peak near

$Q_{c1} = 2\pi/d \approx 1.38$ Å^{-1} evolves continuously and, on further cooling, a second minor peak appears near 50 K at $Q_{c2} \sim 1.7$ Å^{-1}. These most significant changes in the scattering pattern $S(Q)$ occur near the same temperature, at which we observe the appearance of the second hyperfine field in Mössbauer spectroscopy. The peaks are not resolution limited; at 1.2 K, the width of the peak at Q_1 fitted by a Lorentzian yields an exponential decay length of 13.7(8) Å for the spin correlations. The deconvolution with the Gaussian resolution function of 0.05 Å^{-1} (FWHM) is taken into account, albeit of negligible importance. The correlation length varies only slightly with temperature decreasing smoothly to 10(1) Å at 100 K. This indicates that no true long-range magnetic ordering takes place, an observation that is surprising in view of the large (negative) Curie-Weiss temperature [Fig. 3(a)]. The suppression of long-range order, most likely by the geometrical frustration of the magnetic sites due to the tetrahedral coordination, is certainly one of the strongest observed so far, and can be described by a frustration parameter $f > |\theta_{CW}|/1.2$ K ~ 1000. Moreover, the comparably low intensity toward small Q reflects that the sum of magnetic moments of neighboring spins is close to zero and in accordance with strong antiferromagnetic exchange. Although Co^{2+} and Fe^{3+} carry different magnetic moments, the intensity at low Q does not show any indications of uncompensated ferrimagnetic moments.

Whereas the Mössbauer hyperfine field at higher temperatures shows static (Fe-)moments on the kagome sites, a time-dependence of the pair correlation function of these

moments can be inferred from the temperature dependence of the neutron-diffraction data, indicating significant inelastic scattering contributions on a THz-scale at ambient and higher temperatures.[33]

The details of the low temperature magnetic scattering, in particular the exact peak position Q_1 and the more pronounced features in the scattering with the appearance of the second peak at Q_2, differs from the diffuse magnetic scattering observed in the *Swedenborgite* Y$_{0.5}$Ca$_{0.5}$BaCo$_4$O$_7$.[17] Therefore, spin correlations within decoupled 2D kagome lattices will not account for the observation; Q_1 is close although, significantly different from the value 1.33 Å^{-1} that is expected for the (2/3,2/3,0) ordering wave vector of the 2D $\sqrt{3} \times \sqrt{3}$ ground state of the kagome antiferromagnet.[34] An alternative description will be further discussed.

D. High-resolution inelastic neutron scattering

The spin dynamics have been further investigated by inelastic neutron backscattering. An overview on the quasielastic scattering $S(Q,E)$ versus temperature has been obtained using the BASIS spectrometer. Quasielastic scattering appears and is best visible between 70 K and 30 K, see Fig. 7(a). The Q-dependence of this quasielastic scattering closely resembles the $S(Q)$ observed in diffraction data measured at DNS. At lower temperatures, all quasielastic scattering narrows into the elastic resolution window of 3.5 μeV (FWHM). As there is no indication of structural relaxation, we attribute this to spin freezing. There is no simple model free separation of
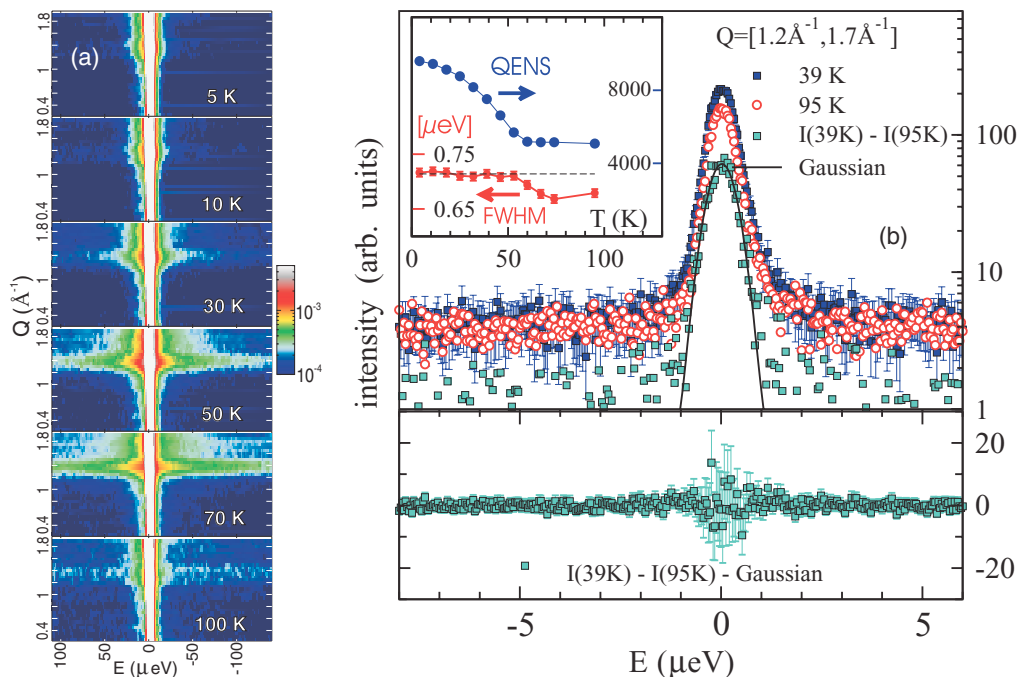

FIG. 7. (Color online) (a) Intensity maps of the scattering $S(Q,E)$ as measured with the backscattering instrument BASIS. For temperatures between 30 K and 70 K, a change of the magnetic quasielastic scattering is observed in the accepted energy range of the instrument with a freezing into the elastic resolution window ($\sim$4 μeV) at low temperature, 10 K. The intensity peaks at the same Q as observed in the diffraction data taken at DNS. (Color scheme is given in log-scale.) (b) Inelastic scattering on SPHERES indicates spin freezing as exemplified by spectra obtained at 95 K and 39 K for Q from 1.2 Å^{-1} to 1.7 Å^{-1}. The difference of these intensities is due to magnetic scattering. The lower part shows the related error bars and the difference to a modeling by a Gaussian on a linear scale (red/dark gray line, 0.80 μeV FWHM). The inset shows the temperature dependence of the integrated quasielastic peak intensity for all measured spectra.

the magnetic signal from the strong elastic intensity to further analyze quantitatively the temperature dependence of the spin correlations.

A complementing study of this apparent freezing transition has been performed at the SPHERES instrument focusing on a narrow dynamic range of ± 10.5 μeV. Measurements were made upon cooling between 93 and 4 K at twelve different temperatures. The quasielastic intensities have been determined by normalization to monitor counts separating a constant background and integrating over a Q-range from 1.2 to 1.7 $\mathring{A}^{-1}$. In this Q-range the change of magnetic scattering intensities with temperature is most significant [inset Fig. 7(b)].

The data measured at 93 K represents essentially nuclear scattering, mostly spin-incoherent scattering from Co. The shape closely resembles the instrumental resolution function to a first-order Gaussian with 0.65 μeV FWHM. Upon cooling the integrated intensity increases, and we note a change toward a slightly larger line width below $\sim$50 K. However, we cannot determine any slow spin relaxation from the spectra. This is exemplified in a more detailed analysis, presented in Fig. 7(b), by focusing on a narrow dynamic range of 6 μeV and showing data in the transition regime at 39 K (magnetic and nuclear) and at 93 K (nuclear); the data at 39 K show a relative increase in peak intensity by a factor 1.38 and can be well described by a Gaussian of 0.72 μeV (FWHM). The difference of the intensities taken at 39 K and 93 K is related to only magnetic scattering from spins, which are freezing in, and is in accordance with the increased Mössbauer hyperfine field observed on the Fe located at the (Co,Fe)1 site. The shape of this magnetic intensity can be modeled by a Gaussian of 0.80 μeV [red line in Fig. 7(b)]. The slight increase in line width compared to the instrumental resolution may still indicate slow spin fluctuations. However, no systematic deviations from the Gaussian modeling of the magnetic intensity appear in the difference plot, which is shown in the lower part of Fig. 7(b). Furthermore, we cannot achieve any significant better description by modeling a possible exponential time decay of spin correlations using a Voigt-profile. These results are qualitatively representative for the spectra taken at other temperatures.

We have further analyzed the line width at low Q, where the Co spin-incoherent scattering gives the dominant contribution. Here one observes a larger increase reaching a line width of 0.82 μeV at low temperatures. The temperature dependence resembles a possible splitting of the Co spin-incoherent scattering due to hyperfine fields acting on the Co nuclei with an onset between 50 and 60 K, coinciding with the Mössbauer $T_{f2} = 55$ K. For low T this hypothesis yields a splitting energy of ± 0.2 μeV, corresponding to a weak hyperfine field of $\sim$7 T. One may note that an apparent broadening due to a splitting of the incoherent scattering may also explain the "constant" line width of the peak intensity below 50 K arising from the superposition of four contributions, each described by the elastic resolution as obtainable from the 95 K data, i.e., three splitted spin incoherent terms and a central magnetic line. Unfortunately the supposed splitting is rather small, actually one and two orders of magnitude less than observed in CoO[35] and $Ho_2Ti_2O_7$,[36] respectively; theoretical estimates of the hyperfine fields are certainly desirable.

Both the BASIS and SPHERES data reveal a rapid change in the spin dynamics, which indicates a dynamically inhomogeneous behavior. A possible explanation could be that instead of a continuous slowing down upon cooling, sequentially more and more spins freeze in. This is in accordance with the DNS data, which are obtained in a coarser energy integration of a few meV. Here, spin correlations develop at low temperatures near 100 K with a significant increase near 50 K, where we also observe anomalies in magnetization with a splitting of FC and ZFC susceptibilities, the onset of Mössbauer hyperfine fields for Fe on the interlayer sites, and the freezing dynamics seen in the high-resolution inelastic neutron scattering. According to these observations, obtained on rather different time scales, we see that when interlayer site moments are getting involved in the spin correlations, this leads to a frozen disordered magnetic structure.

IV. MONTE CARLO SIMULATIONS

Monte Carlo simulations can provide further insight into characteristic spin structures, especially if the structures are more complex than those of ideal magnetic order, and predictions from simple model Hamiltonians can be compared with the measured scattering. Recently[16] spin correlations and effects of geometric frustration in the extended kagome lattice of the *Swedenborgite* structure have been studied based on a classical Heisenberg Hamiltonian

$$H = -\frac{1}{2} \sum_{i,j} J_{i,j} \, \mathbf{S}_i \cdot \mathbf{S}_j,$$

where the exchange J have been confined to nearest-neighbor bonds. A distinction of antiferromagnetic nearest neighbor exchange ($J < 0$) for the in-plane coupling J_{in} between kagome spins and the out-of plane coupling J_{out} between kagome and trigonal layer sites can be made, see Fig. 1(b). Remarkably, as shown by Khalyavin *et al.*,[16] 3D long-range ordered antiferromagnetic ground states do not form if the out-of plane coupling is weaker than the in-plane coupling. Thus, partly ordered states appear for approximately $J_{out}/J_{in} < 1$. Here, we have varied the ratio J_{out}/J_{in} and calculated the scattering cross-section $S(Q)$ to compare them with the neutron scattering data, especially for low temperatures. The simulations, based on a standard Metropolis algorithm, have been carried out in a supercell of $12 \times 12 \times 24$ unit cells with eight different magnetic sublattices, and usual periodic boundary conditions have been used; a larger dimension in c direction has been chosen because of the rather anisotropic decay of the correlations. Typical configurations at low temperatures were obtained by sequential cooling from high temperatures and by performing more than 10^5 Monte Carlo steps per spin. For simplicity and in lack of experimental input, Co and Fe were treated as equal magnetic entities. However, when calculating $S(Q)$ we used the site occupancies as determined from the Mössbauer spectroscopy with spin-only moments 3/2 and 5/2 for Co and Fe, respectively, and included the magnetic form factors.

A first result is that upon varying the ratio of in-plane and out-of plane coupling strength, for $J_{out} = 0.5$ J_{in} the wave-vector dependence of the scattering can be essentially

reproduced for low temperatures. The data shown in Fig. 6(b) correspond to $T = 0.01|J_{in}|/k_B$; a part of the simulated supercell and its spin structure is depicted in the inset. The spin arrangements are not truly long-range ordered in three dimensions. Particularly strong spin correlations along the c-direction are found between the trigonal interlayer sites. In the a-b plane, at least at shorter distances, one may note a typical $120°$ rotation between the spin orientations for neighboring trigonal interlayer sites [see Fig. 6(b), blue spins], which is mediated by neighboring spins on the kagome sites (same figure, red spins). On the other hand, the kagome spins are less ordered along the c-direction, and their projection does not exhibit any clear pattern. The present findings agree well with the previous studies[15,16] for only nearest-neighbor exchange the geometric frustration in the *Swedenborgite* structure promotes strong quasi-1D spin correlations in c-direction. Whereas antiferromagnetically coupled nearest-neighbor spins suffer from geometric frustration resulting in a strong damping of spin correlations in the kagome layers, a ferro-alignment of second neighbors along the polar axis on interlayer sites becomes favorable. However, $YBaCo_4O_7$ has a stronger ordering tendency and equal in-plane and out-of plane coupling strength have been proposed based on simulations. In $YBaCo_3FeO_7$ the out-of plane exchange J_{out} should be weaker. Our Monte Carlo simulations, using a Heisenberg model with $J_{out} = 0.5 \ J_{in}$, show that the observed magnetic scattering and its Q-dependence can be reasonably described and confirm the reported characteristic anisotropy of the spin correlations in the *Swedenborgite* structure.[16]

V. DISCUSSION AND CONCLUSIONS

We have presented a comprehensive study of the magnetic properties of $YBaCo_3FeO_7$, a new compound of the *Swedenborgite* structure, of which we have been able to grow large single crystals by floating zone-mirror technique. High temperature susceptibility measurements between 600 and 1000 K yield a Curie-Weiss temperature estimation of ~ 2000 K related to a strong antiferromagnetic exchange, similar to that observed previously in the other Co-based *Swedenborgites*, i.e., $Y_{0.5}Ca_{0.5}BaCo_4O_7$.[18]

Near 590 K a magnetic anomaly occurs, which we attribute to a cooperative phenomenon due to the continuous and spontaneous change, clearly deviating from the expected paramagnetic behavior. Using single crystals, we found a weak anisotropic susceptibility with a stronger increase upon cooling along the c-axis than in the a-b plane and, for temperatures lower than 590 K, a weak magnetization hysteresis for fields B along the c-direction. Mössbauer spectroscopy reveals the onset of hyperfine field splitting near to this 590 K anomaly in the susceptibility and magnetization measurements. A quantitative analysis reveals that the hyperfine fields are related to the kagome sites. Furthermore, the trigonal interlayer sites experience a hyperfine field splitting at much lower temperatures, below ~ 50 K. Such a large difference in the temperature at which a hyperfine field appears on two different sites in the same structure is rare. In the $Fe^{2+}Fe_2^{3+}F_8(H_2O)_2$ weak ferromagnet, for example, the Fe^{3+} spins order at 157 K, whereas the Fe^{2+} spins remain idle and order only at ~ 35 K, i.e., at five times lower temperature.[37] This idle

spin behavior of the Fe(II) spins was seen as an attempt of the system to minimize the frustration by maintaining these spins in a paramagnetic state.[34] In the title compound, all Fe is trivalent; no true long-range order appears, and the ratio in the temperatures for appearance of local magnetism is even larger, ~ 10. The idle-spin behavior of the interlayer sites between 590 and 50 K might in this respect also be seen as a way to minimize the frustration. In addition the Co- and Fe-site occupancies could be determined from the Mössbauer spectral weights. Accordingly, Fe occupies preferentially the trigonal (Fe,Co-1) site to 82(2)% and the kagome sites (Fe,Co-2) only to 6(1)%. As Mössbauer spectroscopy is a local probe, the appearance of hyperfine fields cannot be taken as an indication of magnetic order. The neutron-diffraction experiments indeed reveal that the system does neither order at such high temperature as 590 K nor order at very low temperatures.

Although it seems likely that there is a common origin of the susceptibility anomaly, the weak anisotropic magnetization and the hyper-fine field, the origin is not yet clear. Such susceptibility anomalies have also been observed in $YBaCo_4O_7$ at 313 K and were in that case related to a structural phase transition from trigonal to orthorhombic symmetry. A structural transition is also found in the *Swedenborgite* $YbBaCo_4O_7$.[38] There are, however, no indications of orthorhombicity in $YBaCo_3FeO_7$. Another speculation to pursue in view of the anisotropy is an orbital-ordering transition involving the kagome sites, which in combination with symmetry allows for DM interactions and might explain the observed weak ferromagnetism.

Interestingly, by Mössbauer spectroscopy we can also distinguish a rather different magnetic behavior of the two different sites: the kagome and interlayer sites. The development of hyperfine fields at the interlayer sites below approximately 50 K coincides well with the freezing of spin correlations, at least within the high resolution of neutron back-scattering spectroscopy. Neutron diffraction has been applied in combination with polarization analysis for an accurate separation of the magnetic-scattering signal. The change of the magnetic-scattering intensity versus temperature can be related to the development of hyperfine fields on the interlayer sites. With respect to Mössbauer spectroscopy, the onset of intensity changes in neutron diffraction takes place at higher temperature due to the shorter probe times. The observed peaks of the magnetic scattering remain significantly broadened compared to the instrumental resolution and do not give any evidence for long-range order even down to lowest temperatures of 1.2 K. Both details of wave-vector dependence of magnetic scattering and the obvious participation of interlayer spins require that the spin correlations extend throughout the 3D magnetic sublattice rather than be confined to two dimensions on independent kagome sheets, as has been proposed earlier for $Y_{0.5}Ca_{0.5}BaCo_4O_7$.[17] Both systems do not show magnetic long-range order at low temperatures; however, there are significant differences in the scattering pattern indicating also differences in the spin correlations. Whereas in the present study of $YBaCo_3FeO_7$ Fe-Mössbauer spectral results clarify the situation, single-crystal neutron diffraction is still needed to prove whether $Y_{0.5}Ca_{0.5}BaCo_4O_7$ is the ideal kagome system as proposed. In this context it is of particular interest to compare the magnetic scattering to

calculations based on simple Heisenberg models, as presented recently.[16] From these calculations one may conclude that the ordering in the pure Co-based system $YBaCo_4O_7$ is on one hand near to degeneracy for all zone-boundary wave vectors, favoring a disordered ground state, and is on the other hand close to a selection of a single wave vector, the K-point, leading to a 3D-ordered phase. The fragile phase stability at least within nearest-neighbor interaction Heisenberg models may also explain the inconsistencies in details of the reported magnetic structure,[12,13,15–17] apart from the known sensitivity to the oxygen stoichiometry.[39]

By Monte Carlo simulations we obtain a reasonable modeling of the magnetic scattering from $YBaCo_3FeO_7$ by using a classical Heisenberg Hamiltonian with antiferromagnetic nearest-neighbor interactions, which are half as strong between kagome and interlayer neighbors as compared to the interaction between only kagome sites, $J_{out} = 0.5\ J_{in}$. A characteristic feature of the spin correlations in the model system is the appearance of strong 1D spin correlations parallel to the c-axis and involving the trigonal interlayer sites, a feature which originates from the specific geometric frustration in the *Swedenborgite* structure.[15,16] This picture seems to apply well to $YBaCo_3FeO_7$, at least at temperatures below $\sim$50 K, whereas at higher temperatures the interlayer spins will fluctuate more rapidly than the kagome spins, which is not expected from Monte Carlo simulations of the used Heisenberg model. The apparently vanishing molecular field (MF) exerted by the kagome neighbor spins onto the interlayer spins at higher temperature may indicate the possible relevance of DM-type interactions; a canting between kagome and interlayer spins should reduce in particular the MF on the interlayer site. We believe that the discussed Heisenberg model with $J_{out} = 0.5\ J_{in}$ reproduces the essential feature of unusual anisotropic spin correlations at low temperatures, however, it has to be considered as a most simple and preliminary model. One may note that according to this model that implies strongly anisotropic spin correlations for the *Swedenborgite* structure, the estimates for an average correlation length obtained from the powder scattering are less meaningful, since the case of partial order and quasi-1D order is rather difficult to distinguish from a disordered state with isotropic short-range correlations only. The observed change in the spin dynamics also seems to have its origin in the easy formation of quasi-1D ordered domains, whereas a further 3D ordering is blocked by the requested reorientation of the whole domains. Future input from single crystal data will help to establish a more realistic description.

*valldor@ph2.uni-koeln.de

[1] C. Castelnovo, R. Moessner, and S. L. Sondhi, Nature **451**, 42 (2008).

[2] T. Fennell, P. P. Deen, A. R. Wildes, K. Schmalzl, D. Prabhakaran, A. T. Boothroyd, R. J. Aldus, D. F. McMorrow, and S. T. Bramwell, Science **326**, 415 (2009).

[3] D. J. P. Morris, D. A. Tennant, S. A. Grigera, B. Klemke, C. Castelnovo, R. Moessner, C. Czternasty, M. Meissner, K. C. Rule, J.-U. Hoffmann, K. Kiefer, S. Gerischer, D. Slobinsky, and R. S. Perry, Science **326**, 411 (2009).

[4] M. P. Shores, E. A. Nytko, B. M. Bartlett, and D. G. Nocera, J. Am. Chem. Soc. **127**, 13462 (2005).

[5] Z. Hiroi, H. Masafumi, N. Kobayashi, M. Nohara, H. Takagi, Y. Kato, and M. Takigawa, J. Phys. Soc. Jpn. **70**, 3377 (2001).

[6] C. Broholm, G. Aeppli, G. P. Espinosa, and A. S. Cooper, Phys. Rev. Lett. **65**, 3173 (1990).

[7] B. Fåk, F. C. Coomer, A. Harrison, D. Visser, and M. E. Zhitomirsky, Euro. Phys. Lett. **81**, 17006 (2008).

[8] G. Aminoff, Z. Kristallogr. **60**, 262 (1924).

[9] G. Aminoff and R. Blix, Kgl. Sv. Vet. H. **11**, 1 (1933).

[10] L. Pauling, H. P. Klug, and A. N. Winchell, Am. Mineral. **20**, 492 (1935).

[11] M. Valldor, Y. Sanders, and W. Schweika, J. Phys.: Conf. Ser. **145**, 012076 (2009).

[12] L. C. Chapon, P. G. Radaelli, H. Zheng, and J. F. Mitchell, Phys. Rev. B **74**, 172401 (2006).

[13] M. Soda, Y. Yasui, T. Moyoshi, M. Sato, N. Igawa, and K. Kakurai, J. Phys. Soc. Jpn. **75**, 054707 (2006).

[14] M. Valldor and M. Andersson, Solid State Sci. **4**, 923 (2002).

[15] P. Manuel, L. C. Chapon, P. G. Radaelli, H. Zheng, and J. F. Mitchell, Phys. Rev. Lett. **103**, 037202 (2009).

[16] D. D. Khalyavin, P. Manuel, J. F. Mitchell, and L. C. Chapon, Phys. Rev. B **82**, 094401 (2010).

[17] W. Schweika, M. Valldor, and P. Lemmens, Phys. Rev. Lett. **98**, 067201 (2007).

[18] M. Valldor, Solid State Sci. **8**, 1272 (2006).

[19] N. D. Mermin and H. Wagner, Phys. Rev. Lett. **17**, 1133 (1966).

[20] K. Binder and A. P. Young, Rev. Mod. Phys. **58**, 801 (1986).

[21] J. R. Stewart, G. Ehlers, H. Mutka, P. Fouquet, C. Payen, and R. Lortz, Phys. Rev. B **83**, 024405 (2011).

[22] M. Valldor, Solid State Sci. **6**, 251 (2004).

[23] F. Laves and H. J. Wallbaum, Z. Anorg. Allg. Chem. **243**, 69 (1939).

[24] N. Hollmann, Z. Hu, M. Valldor, A. Maignan, A. Tanaka, H. H. Hsieh, H.-J. Lin, C. T. Chen, and L. H. Tjeng, Phys. Rev. B **80**, 085111 (2009).

[25] W. Schweika and P. Böni, Physica B **297**, 155 (2001).

[26] O. Schärpf and H. Capellmann, Phys. Stat. Sol. **135**, 359 (1993).

[27] E. Mamontov, M. Zamponi, S. Hammons, W. S. Keener, M. Hagen, and K. W. Herwig, Neutron News **19**, 22 (2008).

[28] [www.jcns.info/jcns_spheres]; W. Häußler, O. Holderer, T. Unruh, and J. Wuttke, Neutron News **22**, 24 (2011).

[29] I. Dzyaloshinsky, J. Phys. Chem. Solids **4**, 241 (1958).

[30] T. Moriya, Phys. Rev. **120**, 91 (1960).

[31] P. Karen, P. M. Woodward, J. Lindén, T. Vogt, A. Studer, and P. Fischer, Phys. Rev. B **64**, 214405 (2001).

[32] D. Vandormael, F. Grandjean, and D. Hautot, G. J. Long. J. Phys.: Cond. Matter **13**, 1759 (2001).

[33] Inelastic scattering also becomes apparent in diffraction mode when using polarization analyzers with different bandpass in energy at the same Q, an observation we have made particularly above ambient temperature.

[34] J. N. Reimers and A. J. Berlinsky, Phys. Rev. B **48**, 9539 (1993).

[35] T. Chatterji and G. J. Schneider, Phys. Rev. B **79**, 212409 (2009).

[36] G. Ehlers, E. Mamontov, M. Zamponi, K. C. Kam, and J. S. Gardner, Phys. Rev. Lett. **102**, 016405 (2009).

[37] M. Leblanc, G. Ferey, Y. Calage, and R. De Pape, J. Solid State Chem. **53**, 360 (1984).

[38] A. Huq, J. F. Mitchell, H. Zheng, L. C. Chapon, P. G. Radaelli, K. S. Knight, and P. W. Stephens, J. Solid State Chem. **179**, 1136 (2006).

[39] Y. Jia, H. Jiang, M. Valkeapää, H. Yamauchi, M. Karppinen, and E. I. Kauppinen, J. Am. Chem. Soc. **131**, 4880 (2009).